Conception of Stretchable Resistive Memory Devices Based on Nanostructure-Controlled Carbohydrate-*block*-Polyisoprene Block Copolymers

Chih-Chien Hung, Yu-Cheng Chiu, Hung-Chin Wu, Chien Lu, Cécile Bouilhac, Issei Otsuka, Sami Halila, Redouane Borsali, Shih-Huang Tung,* and Wen-Chang Chen**

It is discovered that the memory-type behaviors of novel carbohydrate-*block*-polyisoprene (MH-*b*-PI) block copolymers-based devices, including write-once-read-many-times, Flash, and dynamic-random-access-memory, can be easily controlled by the self-assembly nanostructures (vertical cylinder, horizontal cylinder, and order-packed sphere), in which the MH and PI blocks, respectively, provide the charge-trapping and stretchable function. With increasing the flexible PI block length, the stretchability of the designed copolymers can be significantly improved up to 100% without forming cracks. Thus, intrinsically stretchable resistive memory devices (polydimethylsiloxane(PDMS)/carbon nanotubes(CNTs)/MH-*b*-PI thin film/Al) using the MH-*b*-PI thin film as an active layer is successfully fabricated and that using the MH-*b*-$PI_{12.6k}$ under 100% strain exhibits an excellent ON/OFF current ratio of over 10^6 (reading at −1 V) with stable V_{set} around −2 V. Furthermore, the endurance characteristics can be maintained over 500 cycles upon 40% strain. This work establishes and represents a novel avenue for the design of green carbohydrate-derived and stretchable memory materials.

1. Introduction

Stretchable electronics have attracted extensive research interest in wearable electronics, e-skin, and biomedical applications.[1–14] We are particularly interested in stretchable electronics for the applications of transistors,[9,10] memories,[11] light-emitting diodes,[15–17] sensors,[1,4,7,12,18] and solar cells.[19] Among them, organic memory has been considered as basic elements in stretchable information devices. In particular, polymer-based memory devices have shown their advantages for applications because of the low fabrication cost, solution processability, flexibility, high mechanical strength, and good scalability.[20–31] On the other hand, the versatile memory behaviors, including volatile or nonvolatile digital memories such as dynamic-random-access-memory (DRAM), static-random-access-memory, and write-once-read-many-times (WORM), of polymer-based devices could be manipulated through the donor/acceptor characteristics or the nanostructures of the polymer active layer.[32–35] However, to the best of our knowledge, stretchable electronic polymers using carbohydrate-based polymers for the resistive memory application have not been reported yet.

Indeed, oligo- and polysaccharides are interesting hydrophilic biopolymers because they are abundant, renewable, biodegradable, and biocompatible biobased materials such as starch, cellulose, chitin, and chitosan. As it has been shown in recent years, one of the major breakthroughs on carbohydrate-based block copolymer systems is their ability to form nanostructured thin films with high resolution (sub-10 nm domain spacing).[36–40] Lee and coworkers investigated the resistive switching memory devices using chitosan or starch as the active layer.[41,42] Our group also reported the high-performance organic field-effect-transistor

C.-C. Hung, Prof. S.-H. Tung
Institute of Polymer Science and Engineering
National Taiwan University
Taipei 10617, Taiwan
E-mail: shtung@ntu.edu.tw
Prof. Y.-C. Chiu
Department of Chemical Engineering and Materials Science
Yuan Ze University
Taoyuan 32003, Taiwan
Dr. H.-C. Wu, Dr. C. Lu, Prof. W.-C. Chen
Department of Chemical Engineering
National Taiwan University
Taipei 10617, Taiwan
E-mail: chenwc@ntu.edu.tw
Dr. C. Bouilhac
Institut Charles Gerhardt
Université Montpellier
34095 Montpellier Cedex 5, France
Dr. I. Otsuka, Dr. S. Halila, Dr. R. Borsali
Grenoble Alpes University
CNRS
CERMAV UPR 5301, 38041 Grenoble Cedex 9, France
E-mail: borsali@cermav.cnrs.fr

DOI: 10.1002/adfm.201606161

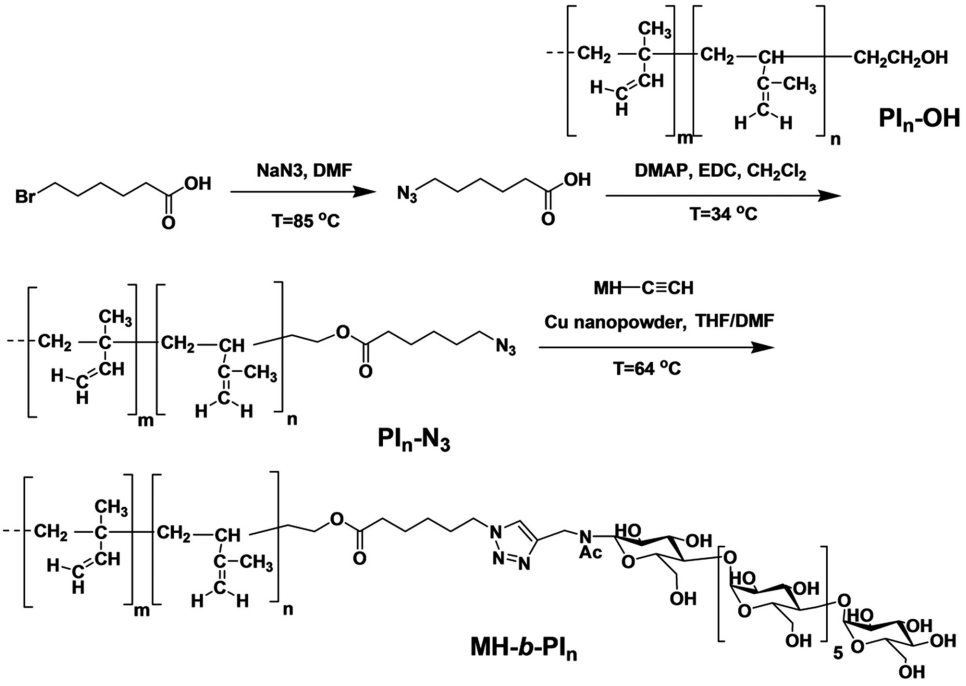

Scheme 1. Synthesis of maltoheptaose-*block*-polyisoprene (MH-*b*-PI$_n$) block copolymers.

memory device using oligosaccharides[43] and their block copolymers,[44–46] in which the hydroxyl moiety could trap the electrons and serve as the charge-trapping element. However, the carbohydrate-based materials inhere the capability to regulate charges but lack elastic properties due to the strong hydrogen bonding. While polyisoprene (PI) is a well-known neutral rubber with a relative low glass transition temperature (T_g) of –72 °C, the shape of polyisoprene-based materials can be recovered after being stretched or deformed. One advantage of introducing the PI in block copolymer system is that the nonstretching moiety can spontaneously assemble into nanodomains by controlling Flory–Huggins interaction parameters between both PI and MH blocks. Therefore, it would be interesting to take the advantages of oligosaccharides and polyisoprene on preparing block copolymers for stretchable memory devices.

Herein, we report new stretchable diblock copolymers, maltoheptaose-*block*-polyisoprene (MH-*b*-PI) consisting of hydrophilic oligosaccharides, (MH) block, and rubber-based PI block for charge-trapping capability and stretchable property, respectively. The well-controlled nanostructure and intrinsic morphology of MH-*b*-PI thin film upon stretching were determined using atomic force microscopy (AFM), grazing-incidence small-angle X-ray scattering (GISAXS), and scanning electron microscope (SEM). To the best of our knowledge, this is the first example of integrating stretchable carbohydrate block copolymers-based materials into the electrical memory device of the polydimethylsiloxane(PDMS)/carbon nanotubes(CNTs)/MH-*b*-PI thin film/Al configuration, where the relationship between the nanostructure, memory characteristics, and stretching behaviors was explored.

2. Results and Discussion

2.1. Synthesis and Characterization of MH-*b*-PI Block Copolymers

As outlined in **Scheme 1**, a click reaction occurs using an alkyne-functionalized maltoheptaose (MH—C≡CH) with two azido-terminated polyisoprenes (PI$_n$-N$_3$) differentiated by their molecular weight. Note that the synthetic procedure of monomers, precursors (MH—C≡CH and PI$_n$-N$_3$), and their characterization are all detailed in Figures S1–S3 (Supporting Information).

The achievement of the click reactions for MH-*b*-PI$_{12.6k}$ was confirmed by the disappearance of the signal at 2096 cm^{-1}, assigned to the azido group of PI$_n$-N$_3$, in infrared spectra (IR) (Figure S3a, Supporting Information). The corresponding ^{1}H NMR spectrum in **Figure 1** exhibits the presence of the protons characteristic of both the PI$_n$ and MH blocks together with the characteristic signal of proton of the triazole ring at δ = 8.12 and 7.89 ppm. In the size-exclusion chromatography (SEC) (Figure S4,Supporting Information) that used tetrahydrofuran (THF) solvent as the eluent, the retention volumes of MH-*b*-PI$_n$ are slightly larger than those of their precursors PI$_n$-N$_3$, which apparently indicates a decrease of molecular weights. This phenomenon observed on SEC traces may be due to aggregation or self-assembly of the amphiphilic copolymers in THF since THF is not a good solvent for maltoheptaose block. A similar observation has already been reported in the literature.[47] The above results suggest the successful preparation of the targeted MH-*b*-PI block copolymers. The polymer with a shorter PI block, MH-*b*-PI$_{3.8k}$, also exhibits the same results on NMR and SEC spectra, as detailed in the Supporting Information.

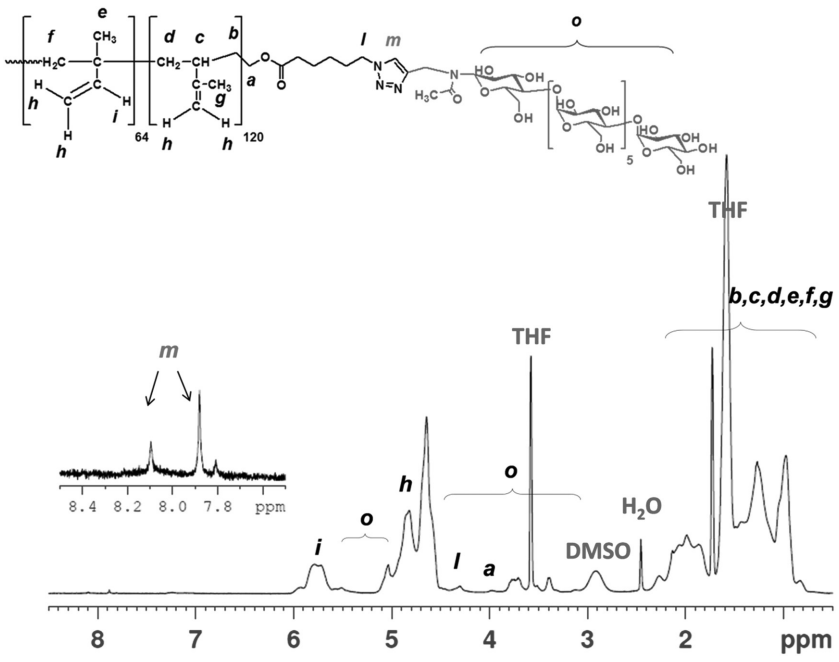

Figure 1. ^{1}H NMR spectrum (400 MHz; THF-d^8 and six drops of DMSO-d^6) of MH-*b*-$PI_{12.6k}$.

along q_y axis (Figure 2e), which is expected for the cylinders parallel to the surface in thin films. The results reveal that the orientation of cylindrical domains changes from perpendicular to parallel by increasing the annealing time, and the *d*-spacing of the perpendicular and parallel cylinders are 13.6 and 13.2 nm, respectively. The main reason for the orientation change may be due to the low solubility of MH in THF as well as the different volatility between THF and water that results in varying vapor compositions with time. With a shorter annealing time (8 h), THF is the major component in the vapor because of its high volatility. Since THF is a selective solvent to PI block, the PI matrix may swell more than MH domains under solvent annealing such that MH tends to form spheres when THF diffuses into the film. When the solvent evaporates as the annealing is terminated, the film thickness is greatly reduced and the MH spheres may join one another along the thickness direction, thus leading to the formation of the perpendicular cylindrical arrays. As the annealing time extends to 48 h, more water diffuses into films to swell the MH domains. The MH spheres are thus transformed into cylinders. In general, the high surface tension MH blocks tend to contact substrate while the low surface-tension PI block tend to expose to air, which thus forces the MH cylinders to be parallel to the surface to minimize the surface free energy.

2.2. Nanostructured Morphology of MH-*b*-PI Thin Films

The thin films of MH-*b*-$PI_{3.8k}$ (f_{PI} = 0.76) and MH-*b*-$PI_{12.6k}$ (f_{PI} = 0.95) with the thickness of 50–55 nm were spin coated from a THF solution, a poor solvent for MH block, onto bare Si wafer and solvent-annealed under the mixture of THF/H_2O = 1:1 (w/w) for 0–48 h. The surface structure of the MH-*b*-PI thin films was characterized using AFM (**Figure 2** and Figures S5 and S6, Supporting Information). The as-cast MH-*b*-$PI_{3.8k}$ thin film shows a random spherical structure but turns into hexagonal close-packed dots and a fingerprint-like structure with increasing the annealing time to 8 and 48 h, respectively. On the other hand, the MH-*b*-$PI_{12.6k}$ thin film exhibits random and ordered spherical structures for the as-cast and 24 h annealing conditions (Figure S6a, Supporting Information; Figure 2c). These results indicate that the distinct changes on nanostructured morphologies can be achieved by the design of asymmetric architecture of block copolymer with dia fferent fraction of MH blocks in a soft matrix of PI blocks.

To gain more insight into the morphology and orientation, the sample was subsequently analyzed using GISAXS experiments. Figures S7 and S8 (Supporting Information) show the ring-like patterns for both as-cast MH-*b*-$PI_{3.8k}$ and MH-*b*-$PI_{12.6k}$ thin films, indicating that MH microdomains are randomly oriented. The *d*-spacing values determined by the relation $d = 2\pi/q^*$ are 13.8 and 12.8 nm, respectively. After annealing for 8 h, the structure in MH-*b*-$PI_{3.8k}$ thin film becomes more ordered and oriented, and thus higher-order scattering peaks at $\sqrt{3}q^*$ and $2q^*$ appear along the q_y axis as shown in Figure 2d. This ratio of the peak positions implies the formation of cylinders standing on the substrate with a hexagonal close packing. The dots in the AFM image of Figure 2a are therefore the cross-sections of the perpendicular cylinders. After 48 h annealing, the higher order scattering peaks turn to be at $2q^*$ and $3q^*$

In the case of MH-*b*-$PI_{12.6k}$ films, since the volume fraction of MH blocks is rather low, MH blocks always form spherical domains regardless of annealing time, although the structure becomes more ordered after annealing, as evidenced by the q^* and $\sqrt{2}q^*$ scattering peaks of the ordered body-centered cubic (BCC) spherical domains with *d*-spacing of 12.5 nm after annealing for 24 h (Figure 2f). These ordered nanostructures as well as the *d*-spacing of phase separation are both important factors to affect the charge-trapping and transporting behaviors for resistive memory devices.

2.3. Resistive Memory Performance Using MH-*b*-PI Nanostructured Thin Films

As shown in **Figure 3**a, the memory devices were fabricated based on ITO/MH-*b*-PI thin film (50 nm)/Al sandwiched structure. The representative current–voltage (*I*–*V*) characteristics for the solvent-annealed thin films are shown in Figure 3b–d. Note that the results are averaged from 20 devices in three different batches. The statistical analysis of 20 devices' performance (including V_{set}, I_{on}, I_{off}, $I_{on/off}$ and yield) for three different types of memory device has been summarized in Table S1 (Supporting Information). The device with 8 h solvent-annealed MH-*b*-$PI_{3.8k}$ (vertical cylindrical) initially exhibits a high resistance state (HRS; OFF state) as the voltage was swept from 0 to −1.4 V (1st sweep); however, the current underwent an abrupt increase at −1.4 V (V_{set}, threshold voltage, LRS; ON state) with an

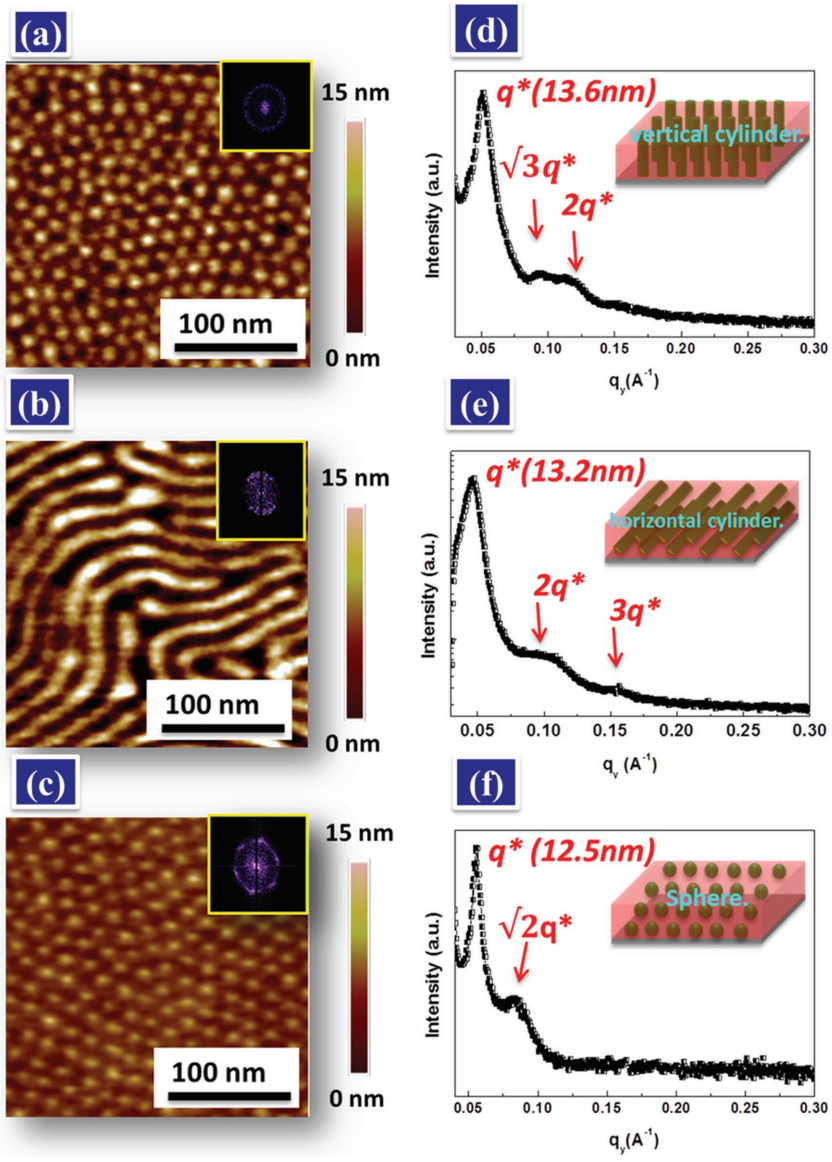

Figure 2. AFM topographies of a) 8 h annealed, b) 48 h annealed MH-*b*-$PI_{3.8k}$, and c) 24 h annealed MH-*b*-$PI_{12.6k}$ thin films. 1D GISAXS profiles of d) 8 h annealed, e) 24 h annealed MH-*b*-$PI_{3.8k}$, and f) 24 h annealed MH-*b*-$PI_{12.6k}$ thin films.

ON/OFF current ratio of 10^5. The operation used to drive HRS to LRS electrical transition is defined as the "SET" or "writing process" process. The device can maintain in the ON state for the subsequent negative sweep from 0 to −4 V (2nd sweep) and positive sweep from 0 to 4 V (3rd sweep). Thus, the device with MH vertical cylinders does not return to the original OFF state even after turning off the power or applying a reverse bias, exhibiting a nonvolatile WORM memory characteristic. In addition, the long-term stability of the device with stable ON and OFF states can be maintained for at least 10^4 s with the ON/OFF ratio over 10^5 at a bias of −1.0 V (Figure 3b). Interestingly, when introducing MH-*b*-$PI_{3.8k}$ thin film with the horizontal-cylinder nanostructure (48 h annealed) as the active layer, the memory behavior is significantly changed. When a negative bias is applied, the current is initially low and suddenly increases at a voltage around −1.7 V. It switches the cell from a high-resistance state (HRS or OFF state) to a low-resistance state (LRS or ON state), and this phenomena is defined as the writing (SET) process (1st sweep). The device then could be maintained at the LRS at subsequent sweep with a negative bias (2nd sweep). As a reverse bias (i.e., positive bias) is applied to the cell in LRS, the memory is turned back to its original HRS with a significant current dropping at ≈3 V (erasing or RESET process) (3rd sweep). Note that this memory device could not be switched ON under a positive bias, even at a voltage as high as 4 V (4th sweep). With inducing a negative bias, on the contrary, the memory could be reprogrammed from the HRS state to the LRS (5th sweep), indicating that the studied device possesses a Flash-type nonvolatile memory behavior.[48–50] Besides, the stable retention time was measured for at least 10^4 s with the ON/OFF ratio of 10^2 at a reading voltage of −1.0 V as illustrated in Figure 3c.

In contrast, the device with the solvent-annealed MH-*b*-$PI_{12.6k}$ thin film (Figure 3d) initially stayed at a HRS and its current level could be gradually changed as applying a negative voltage bias. The memory cell was then switched ON from HRS to LRS at ≈−1.5 V with an ON/OFF ratio of 10^5 (reading at −0.5 V). Such memory device, however, would return back to HRS (OFF state) immediately when the electrical power was turned off. Those electrical characteristics suggest a typical volatile DRAM memory behavior, which is similar to the previous reports.[51,52] It is worth mentioning that the switching threshold voltage (V_{set}) and the deviation of all annealing-based devices can be improved because of the highly order-packed nanostructure, which might stabilize the charge trapping and transport through the vertical direction between top and bottom electrodes, as mentioned in the previous literature.[35] All above results indicate that the switching performance could be enhanced with stable V_{set} around −1.5 V as well as high ON/OFF ratio current by solvent annealing. Note the resistive memory devices work on cross-point arrays of memory cells with the active joint areas of 0.2 × 0.2, 0.4 × 0.4, and 0.6 × 0.6 mm^2, respectively. We have obtained the similar value of current density on different active joint areas and thus the memory performance is independent on cell areas in this study.

2.4. Proposed Mechanism for MH-*b*-PI-Based Memory Behavior

The possible electrical switching mechanism of the MH-*b*-PI-based devices is proposed based on the nanostructure, as described below. Considering the trapping mechanism, the MH

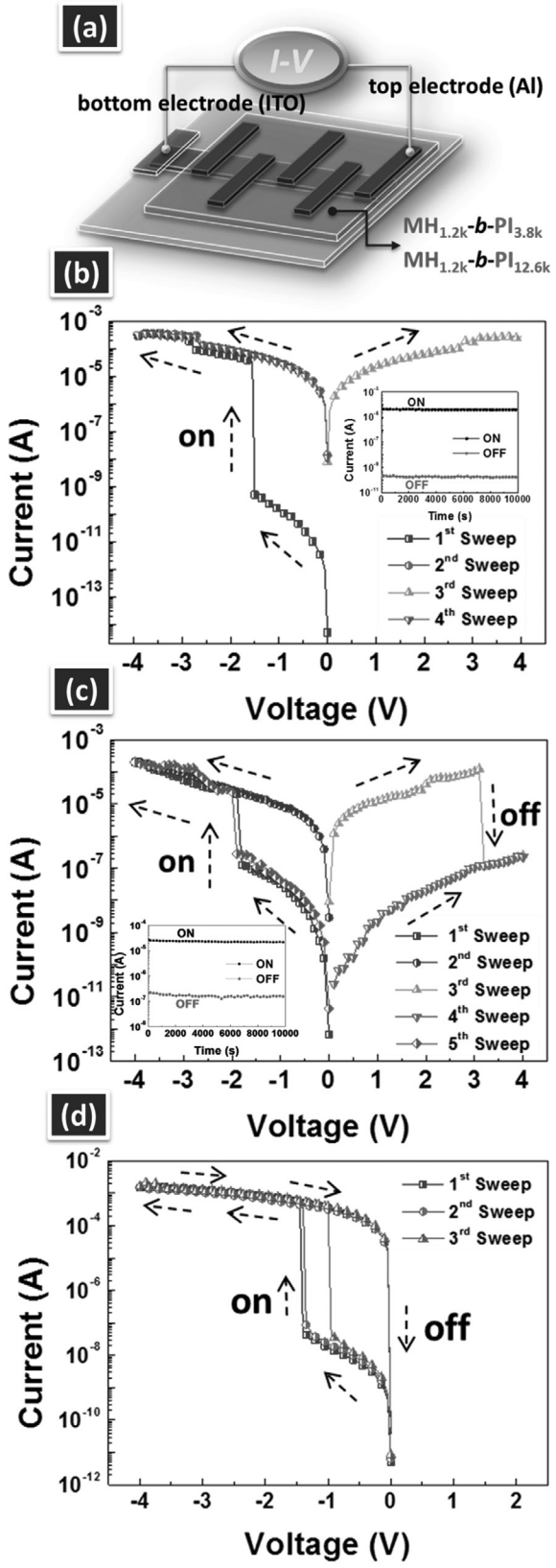

Figure 3. a) ITO/MH-*b*-PI thin film/Al sandwiched structure of resistive memory devices. *I–V* characteristics of the b) 8 h annealed, c) 48 h annealed MH-*b*-$PI_{3.8k}$, and d) 24 h annealed MH-*b*-$PI_{12.6k}$-based devices.

moieties could trap electrons due to the occurrence of protonation on hydroxyl groups via the external electric field-induced electrons.[43] The electrons are gradually trapped on the interface of MH first and then form an active route when saturating, which leads to the switching from the HRS state to the LRS state. In contrast, the PI block serves as an insulating matrix to control the charge trapping through their nanostructures of the block copolymer film.

The annealed MH-*b*-$PI_{3.8k}$ and MH-*b*-$PI_{12.6k}$-based devices exhibit the WORM, Flash, and DRAM-type behaviors for the vertical cylinder, horizontal cylinder, and order-packed sphere nanostructures, respectively. The key factor of dominating the memory behaviors is attributed to the nanostructures and orientation of the MH domain, which serves as charge trapping or transporting segments. As shown in **Figure 4**a, the WORM-type memory of annealed MH-*b*-$PI_{3.8k}$ thin film is observed since the vertically cylindrical MH domain is perpendicular to the electrodes, which directly serves as active routes for charge trapping. However, in the case of the charge trapping on the horizontal MH cylinders, the cylindrical domain separated

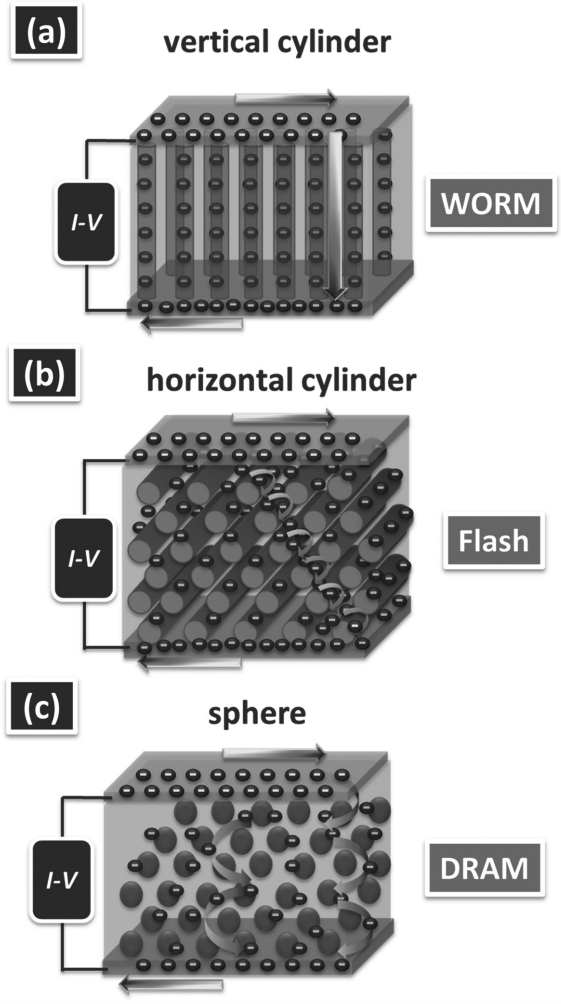

Figure 4. Proposed mechanism for MH-*b*-PI-based memory behavior, including a) WORM (vertical cylinder), b) Flash (horizontal cylinder), and c) DRAM (sphere).

by the PI matrix cannot form an immediate channel connecting the two electrodes and thus the active route may fall away upon applying the reverse bias, showing the Flash-type behavior. (Figure 4b) On the contrary, the DRAM-type behavior is observed on the MH-*b*-$PI_{12.6k}$-based device due to the lower volume fraction of the MH spherical domain, which reduces the trapping capability. Therefore, the proposed oligosaccharides-based block copolymers can successfully switch the memory behaviors including WORM, Flash, and DRAM by tuning the self-assembly nanostructures, showing a great potential for the next generation green electronics.

2.5. Stretchable Resistive Memory Using the MH-*b*-PI Thin Films

2.5.1. Fabrication of the MH-b-PI-Based Stretchable Devices

The rubber-based PI block serves as not only an insulator matrix for phase separation in the block copolymer but also provides the flexible characteristic. For developing wearable and stretchable device applications, we proceeded to fabricate fully stretchable memory devices based on the PDMS substrate/CNTs/MH-*b*-PI thin film/Al configuration shown in **Figure 5**, and the schematic process to fabricate the device is illustrated in **Figure 6**. Rubber-like stretchable conducting PDMS/CNTs composite is used as the bottom electrode,

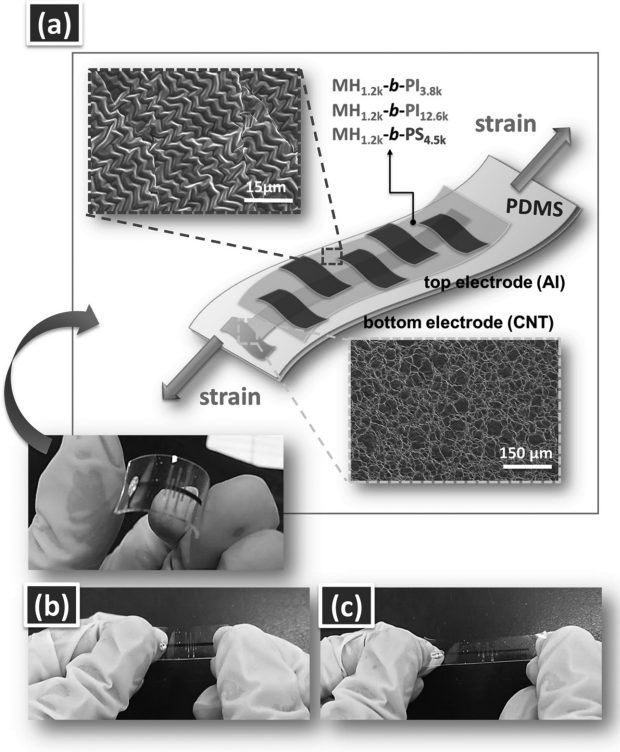

Figure 5. a) Stretchable memory device of PDMS substrate/CNTs/MH-*b*-PI thin film/Al structure. High stretchability of the rubber-based memory devices under b) 0% and c) 100% strains.

which could maintain good conductivity under stretchability over 100%.[53,54] First, the CNTs film was prepared via spray coating on a masked *n*-octadecyltrimethoxysilane (ODTS)-modified Si wafer and subsequently covered with the PDMS mixture (20:1) under 80 °C for curing overnight, and then peeled off. Note that the ODTS is introduced to increase the surface hydrophobicity of the Si substrate. Second, the MH-*b*-PI thin films were transferred onto the PDMS/CNTs substrate and controlled the nanostructures by solvent annealing. Finally, the top electrode (Al) was deposited onto the per-stretched PDMS/CNTs/ MH-*b*-PI films and then released the device in order to preserve the conductivity of metal (Al) during the stretching test.

2.5.2. Morphology of MH-b-PI Thin Films under Stretching Condition

The morphology change of the MH-*b*-PI thin film upon stretching was investigated by scanning electron microscope (SEM). At the same time, MH-*b*-$PS_{4.5k}$ block copolymer where PS blocks are in a rigid glass state at room temperature was prepared to compare with MH-*b*-PI. The three block polymers (MH-*b*-$PI_{3.8k}$, MH-*b*-$PI_{12.6k}$, and MH-*b*-$PS_{4.5k}$) were transferred onto pure PDMS substrate and stretched under 0%–100% strain, as shown in **Figure 7** and Figure S9 (Supporting Information). The wrinkle structures of the three polymer films at the initial state are originated from the wrinkles formed on PDMS surface that occurs during the thermal-crosslinking process in the bounded petri dish. After stretching, no obvious crack even under 100% strain is observed for MH-*b*-$PI_{12.6k}$ thin film in Figure 7e–h, indicating that the higher volume of the rubber-based PI (f_{PI} = 0.95) provides the excellent stretchability. For the case of MH-*b*-$PI_{3.8k}$ thin film, the cracks appear at the 60% strain and become larger over 80% strain. In sharp contrast, the structure of MH-*b*-$PS_{4.5k}$ thin film exhibits few ruptures under 40% strain and then shows critical cracks vertical to the stretch direction under 60%–100% strain. The above results suggest that the stretchability of thin film can be effectively improved with increasing the flexible PI component in the block copolymers.

In addition, the well-controlled nanostructures on the rubber-based memory device were also demonstrated by the GISAXS profiles. **Figure 8**b,c and Figure S10 (Supporting Information) show the 1D and 2D GISAXS profiles of the annealed MH-*b*-$PI_{12.6k}$ thin film onto PDMS substrate and under stretching condition of 0%, 20%, 40%, 60%, 80%, and 100% strain. Note that the samples were transferred back to the bare Si wafer for the GISAXS analysis to avoid the scattering noise from the PDMS substrate. The distinct primary scattering peaks (q^*) with the higher order scattering still exhibit a BCC spherical nanostructure upon stretching, while the *d*-spacing of the MH spheres slightly decreases from 12.4 to 12.2 nm with increasing strain to 100%. It suggests that the deformed PI chains under stress can relax back to original conformation due to the flexible nature and therefore the self-assembly structure of MH-*b*-PI can be maintained after stretching.

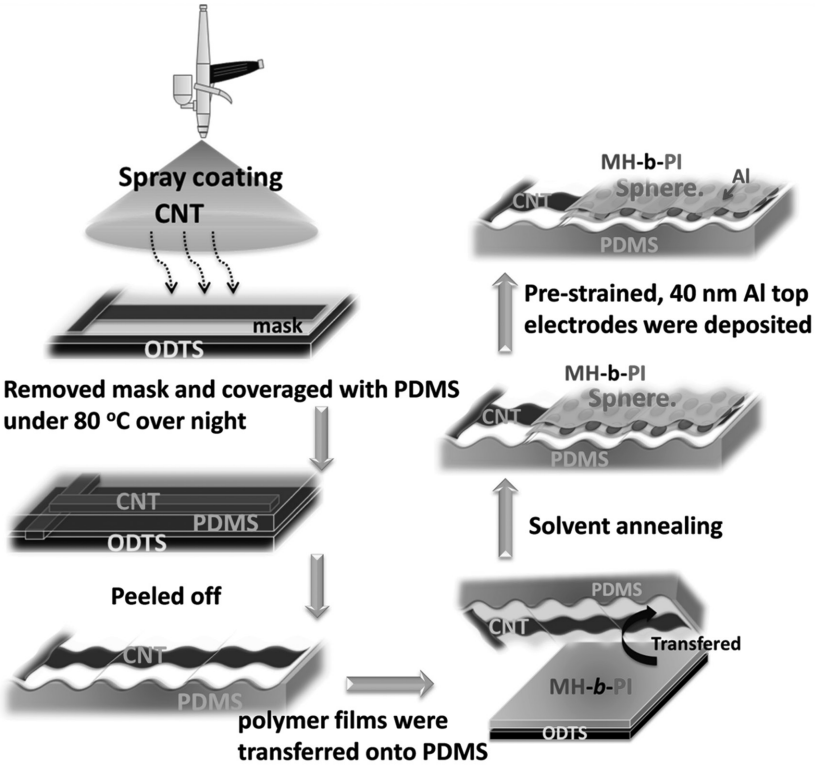

Figure 6. Schematic processes to prepare the rubber-based stretchable devices.

2.5.3. Resistive Memory Performance for MH-b-PI-Based Stretchable Devices

The electrical characteristics of the stretchable memory devices using the block copolymers (MH-*b*-$PI_{12.6k}$) as the active layer were further investigated. Figure 8d shows the current–voltage (*I*–*V*) representative characteristics of the resistive memory devices using MH-*b*-$PI_{12.6k}$ under 0%–100% strain. Similar to the memory property observed on the rigid ITO substrate, the device with MH-*b*-$PI_{12.6k}$ exhibits a DRAM behavior. To clearly study the switching performance upon stretching, the characteristics of ON/OFF current ratio at the reading voltage of –1 V and threshold voltage (V_{set}) as a function of strain are plotted in Figure 8e. All of the ON/OFF current ratios remain similar around 10^6 while the V_{set} is gradually decreased from –3.9 to –2 V with increasing strain. It can be explained by the influence of the film thickness since the polymer film becomes thinner during stretching. Thus, it results in rapid trapping and tends to form an active route between top and bottom electrodes, causing a downtrend of V_{set}.

Moreover, we also performed rigorous repeated stretching cycle tests to determine the stability by subjecting the device to 1000 cycles of continuous stretch-relaxation with 40% strain (Figures S11 and S12, Supporting Information). Figure 8f shows the ON/OFF current ratio at the reading voltage of –1 V and threshold voltage (V_{set}) after the cycling test for the MH-*b*-$PI_{12.6k}$ device. The stable ON/OFF current ratio of over 10^6 can be kept with the V_{set} around –2 V over 500 cycles, and then decreases slightly over 1000 cycles. These tests demonstrate the excellent stretchability and stable performance of the memory device using the MH-*b*-PI block copolymers as the active layer.

3. Conclusion

In the study, we successfully demonstrate that the resistive memory-type behaviors including WORM, Flash, and DRAM can be significantly tuned by the well-controlled nanostructure (vertical cylinder, horizontal cylinder, and order-packed sphere) of the new synthesized MH-*b*-PI block copolymers. The rod-like MH component and the flexible PI block serve as the charge-trapping site and stretchable matrix, respectively. By this rational design of integrating flexible PI polymer into block copolymer, the stretchability of MH-*b*-PI thin film can be effectively improved by increasing the flexible PI component. In the case of MH-*b*-$PI_{12.6k}$ thin film, no obvious crack is observed even under a 100% strain. Highly stretchable memory devices (PDMS/CNTs/MH-*b*-$PI_{12.6k}$/Al) exhibit an excellent ON/OFF current ratio of over 10^6 (reading at –1 V) with a stable V_{set} around –2 V under 0%–100% strain. Furthermore, the endurance characteristics can be maintained over 1000 cycles upon 40% strain, indicating that the rubber-based block copolymers provide great potential applications for high-performance stretchable and wearable electronic devices.

4. Experimental Section

Materials: *N*-maltoheptaosyl-3-acetamido-1-propyne (MH—C≡CH) was prepared following a reported method.[55] Hydroxyl-terminated polyisoprenes (1,2 and 3,4-addition) (PI_n—OH), with molecular weights (M_n) of 3000 and 12 500 g mol^{-1} and dispersity ($Đ$) of 1.09 and 1.06, respectively (data from supplier), were purchased from Polymer Source, Inc. (Montreal, Quebec, Canada). 6-bromohexanoic acid (Aldrich, 97%), sodium azide (NaN_3, Alfa Aesar, 99%), 4-(dimethylamino) pyridine (Aldrich, ≥99%), 1-(3-dimethylaminopropyl)-3-ethylcarbodiimide hydrochloride (TCI Europe, >98%), and copper nanopowder (Cu(core)/CuO(shell), Alfa Aesar, 99.9%) were used as received. Dry dichloromethane (CH_2Cl_2, ≥99.8%, water content ≤0.001%) was purchased from Aldrich and used as received. Cuprisorb resin was purchased from Seachem (Madison, GA, USA) and used as received. Other reagents and solvents were used without further purification.

Synthesis of MH-b-PI Block Copolymer by Click-Chemistry: The click reactions between PI_n-N_3 and MH—C≡CH were performed in a dimethylformamide (DMF)/THF solvent mixture (1/1.6 v/v) at 64 °C for 2 d in the presence of Cu/CuO as the catalytic system. The use of such heterogeneous copper catalyst was preferred because of the easy catalyst/product separation after reaction via a simple filtration. Besides, Cu/CuO nanoparticles have already proved their efficiency as a catalyst for click azide/alkyne cycloaddition.[56] A slight excess of MH—C≡CH

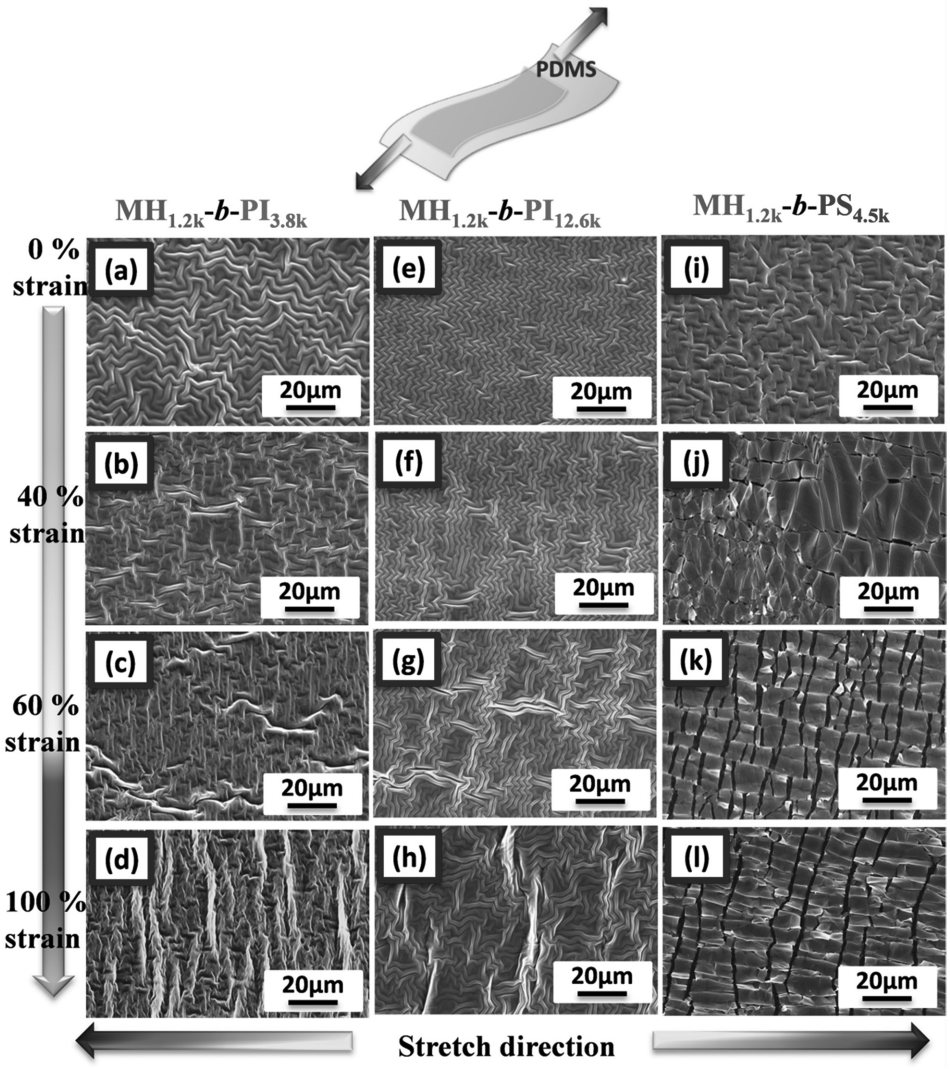

Figure 7. SEM morphology of a–d) MH-*b*-$PI_{3.8k}$, e–h) MH-*b*-$PI_{12.6k}$, and i–l) MH-*b*-$PS_{4.5k}$ thin films under the stretching condition of 0%, 40%, 60%, and 100% strains.

(1.2 equivalent) was used to ensure the complete coupling reactions. The excess of MH—C≡CH was eliminated by precipitation in cold methanol.

Synthesis of Polyisoprene-block-Maltoheptaose ($PI_{12.6}$*-b-MH)*: A solution of s(2.00 g, 0.526 mmol) in THF (24 mL) was degassed by high purity argon for 10 min. The solution was then cannulated to a similarly degassed solution of MH—C≡CH (777 mg, 0.631 mmol) in DMF (15 mL) and copper nanopowder (90.5 mg, 0.631 mmol) was added under an argon atmosphere. The mixture was stirred at 64 °C until the IR spectrum showed the complete disappearance of the signal due to the azido group of $PI_{12.6}$-N_3 precursor (generally 2 d). The reaction mixture was then filtered through Celite and concentrated. To completely remove copper, the concentrate was redissolved in an excess of THF together with a few milliliter of water and charged with cuprisorb resin. The mixture was stirred at 50 °C, filtered through Celite and concentrated by evaporation. The crude product was then purified by precipitation using THF as a good solvent and cold MeOH as the poor solvent. The copolymer was collected by filtration and dried under vacuum to give MH-*b*-$PI_{12.6}$ as a white solid with yield of 73%. ^{1}H NMR (400 MHz, THF-d^8 and six drops of DMSO-d^6) δ (ppm) = 8.08 and 7.86 (2s, H from 1,4-disubtituted triazole), 7.77 (s, H from 1,5-disubtituted triazole), 6.05–5.62 (br, CH_2=C*H*— from the repeating units of PI), 5.50–5.21 (br m, OH from MH), 5.22–4.84 (br m, H-1 from MH), 5.26–4.50 (br m, CH_2= from the repeating units of PI), 4.52–4.39 (br, OH from MH), 4.32 (m, —CH_2—N), 4.32–3.12 (br m, H-2, 3, 4, 5, 6 from MH), 3.92 (br, —CH_2—O—C(=O)—), 2.48–0.52 (br m, aliphatic protons).

Morphology Characterization: For solvent-annealing treatment, thin films were put in a tightly capped 2 L glass bottle containing an uncapped 20 mL beaker filled with a mixture of 2.5 g of THF and 2.5 g of water. The nanostructure of polymer film was obtained with a Nanoscope 3D controller AFM (Digital Instruments) operated in the tapping mode at room temperature. GISAXS was conducted on beamline BL23A1 in the National Synchrotron Radiation Research Center (NSRRC), Taiwan.

Fabrication and Characterization of Resistive Memory Devices: The resistive memory devices were fabricated using the studied copolymers with an ITO/MH-*b*-PI thin film (50 nm)/Al sandwiched structure. The ITO-coated glass substrate was first precleaned by an ultrasonic cleaning process with water, isopropanol, and acetone successively for 15 min each. The studied polymer solution of 10 mg mL^{-1} in chloroform was filtered through a polytetrafluoroethylene filter

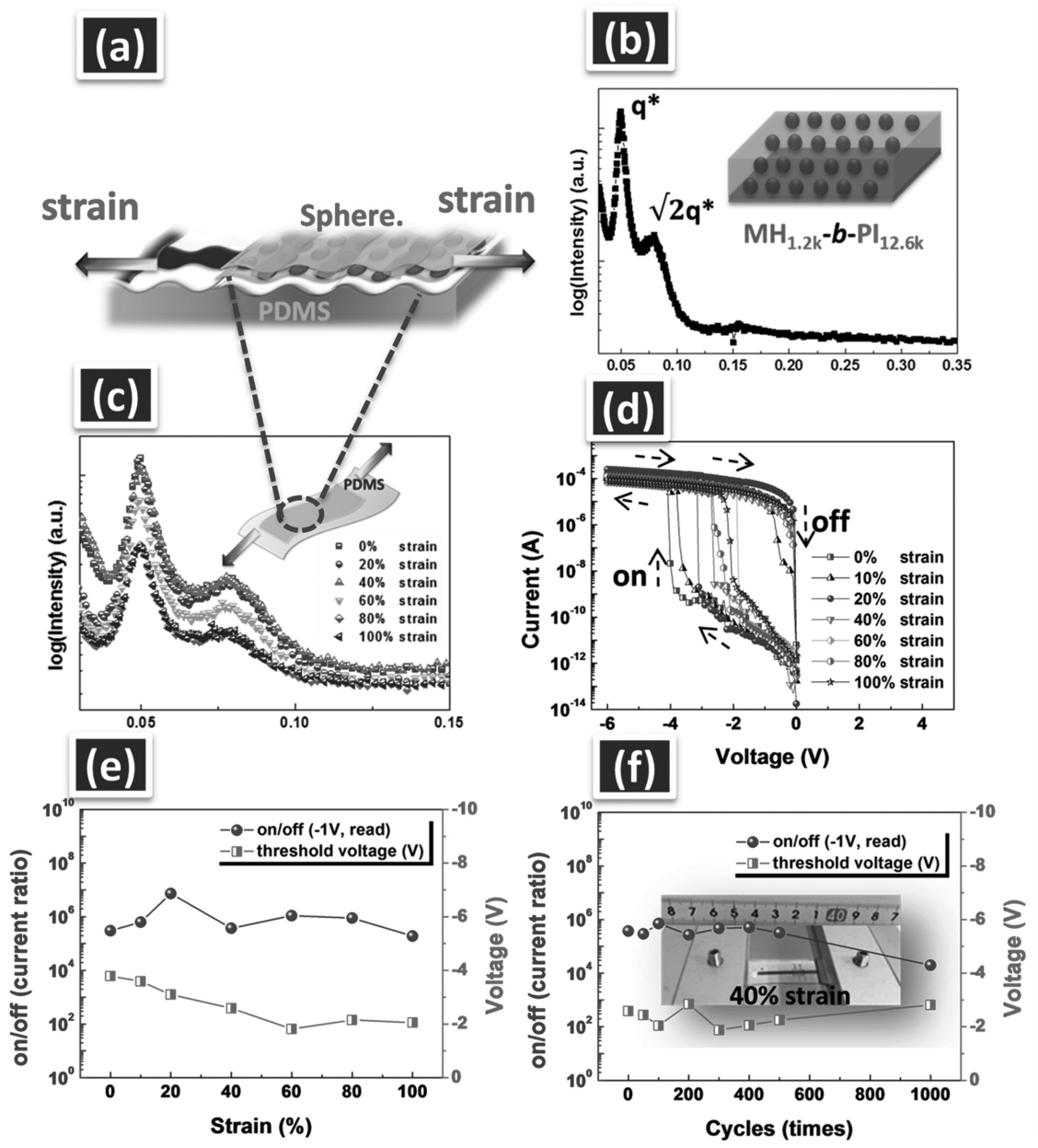

Figure 8. a) Rubber-based resistive memory devices under stretching. 1D GISAXS profiles for b) MH-*b*-$PI_{12.6k}$ thin films on PDMS substrates and c) under stretching conditions at 0%, 20%, 40%, 60%, 80%, and 100% strains. d) Current–voltage (*I*–*V*) characteristics of MH-*b*-$PI_{12.6k}$-based devices under 0%–100% strain. e) Characteristics of ON/OFF current ratio and threshold voltage as function of different stain for the fully stretchable MH-*b*-$PI_{12.6k}$ device. f) The stability of the device for 1000 times stretching cycle at 40% strain.

membrane with 0.22 mm pore size, and then spin-coated onto the ITO substrate at 1000 rpm for 60 s. This process produced active thin films of ≈50 nm, measured with a surface profilometer. In addition, a solvent annealing process (under the mixture of THF/H_2O = 1:1 (w/w) for 0–48 h) was introduced to induce the well-controlled nanostructures and enhance the resistive memory device performance. Finally, 40 nm Al top electrodes were deposited using a thermal evaporator at a pressure of 10^{-7} Torr with a depositing rate of 0.5 Å s^{-1}. The top electrode lines were aligned by a shadow mask and perpendicular to the bottom ITO patterns, leading to cross-point arrays of memory cells with active joint areas of 0.2 × 0.2, 0.4 × 0.4, and 0.6 × 0.6 mm^2, respectively. The current–voltage characteristics of the devices were measured by using a Keithley 4200-SCS semiconductor parameter analyzer (Keithley Instruments Inc., Cleveland, OH) in an N_2-filled glove box.

Supporting Information

Supporting Information is available from the Wiley Online Library or from the author.

Acknowledgements

The authors highly appreciate the financial support from Ministry of Science and Technology of Taiwan. The authors also acknowledge NSRRC, Taiwan, for facilitating the X-ray experiments.

Received: November 22, 2016
Revised: December 14, 2016
Published online: February 6, 2017

[1] M. Amjadi, A. Pichitpajongkit, S. Lee, S. Ryu, I. Park, *ACS Nano* **2014**, *8*, 5154.
[2] T. Cheng, Y. Zhang, W. Y. Lai, W. Huang, *Adv. Mater.* **2015**, *27*, 3349.
[3] S. Choi, J. Park, W. Hyun, J. Kim, J. Kim, Y. B. Lee, C. Song, H. J. Hwang, J. H. Kim, T. Hyeon, D.-H. Kim, *ACS Nano* **2015**, *9*, 6626.
[4] A. Chortos, J. Liu, Z. Bao, *Nat. Mater.* **2016**, *15*, 937.
[5] H. H. Chou, A. Nguyen, A. Chortos, J. W. F. To, C. Lu, J. Mei, T. Kurosawa, W.-G. Bae, J. B. H. Tok, Z. Bao, *Nat. Commun.* **2015**, *6*, 8011.
[6] Y. Huang, M. Zhong, Y. Huang, M. Zhu, Z. Pei, Z. Wang, Q. Xue, X. Xie, C. Zhi, *Nat. Commun.* **2015**, *6*, 10310.
[7] B. U. Hwang, J. H. Lee, T. Q. Trung, E. Roh, D. I. Kim, S. W. Kim, N. E. Lee, *ACS Nano* **2015**, *9*, 8801.
[8] S. Jung, S. Hong, J. Kim, S. Lee, T. Hyeon, M. Lee, D. H. Kim, *Sci. Rep.* **2015**, *5*, 17081.
[9] H. C. Wu, C. C. Hung, C. W. Hong, H.-S. Sun, J.-T. Wang, G. Yamashita, T. Higashihara, W. C. Chen, *Macromolecules* **2016**, *49*, 8540.
[10] H. C. Wu, S. J. Benight, A. Chortos, W. Y. Lee, J. Mei, J. W. F. To, C. Lu, M. He, J. B. H. Tok, W. C. Chen, Z. Bao, *Chem. Mater.* **2014**, *26*, 4544.
[11] J. T. Wang, K. Saito, H. C. Wu, H. S. Sun, C. C. Hung, Y. Chen, T. Isono, T. Kakuchi, T. Satoh, W. C. Chen, *NPG Asia Mater.* **2016**, *8*, e298.
[12] C. Wang, X. Li, E. Gao, M. Jian, K. Xia, Q. Wang, Z. Xu, T. Ren, Y. Zhang, *Adv. Mater.* **2016**, *28*, 6640.
[13] K. Xie, B. Wei, *Adv. Mater.* **2014**, *26*, 3592.
[14] C. Yan, W. Kang, J. Wang, M. Cui, X. Wang, C. Y. Foo, K. J. Chee, P. S. Lee, *ACS Nano* **2014**, *8*, 316.
[15] J. Liang, L. Li, D. Chen, T. Hajagos, Z. Ren, S.-Y. Chou, W. Hu, Q. Pei, *Nat. Commun.* **2015**, *6*, 7647.
[16] D. Choi, H. Kim, N. Persson, P.-H. Chu, M. Chang, J. H. Kang, S. Graham, E. Reichmanis, *Chem. Mater.* **2016**, *28*, 1196.
[17] Y. Lee, M. Shin, K. Thiyagarajan, U. Jeong, *Macromolecules* **2016**, *49*, 433.
[18] M. Amjadi, K. U. Kyung, I. Park, M. Sitti, *Adv. Funct. Mater.* **2016**, *26*, 1678.
[19] D. J. Lipomi, B. C. K. Tee, M. Vosgueritchian, Z. Bao, *Adv. Mater.* **2011**, *23*, 1771.
[20] Q. D. Ling, D. J Liaw, C. X. Zhu, D. S. H. Chan, E. T. Kang, K. G. Neoh, *Prog. Polym. Sci.* **2008**, *33*, 917.
[21] P. Heremans, G. H. Gelinck, R. Muller, K. J. Baeg, D. Y. Kim, Y. Y Noh, *Chem. Mater.* **2011**, *23*, 341.
[22] C. L. Liu, W. C. Chen, *Polym. Chem.* **2011**, *2*, 2169.
[23] S. G. Hahm, N. G. Kang, W. Kwon, K. Kim, Y. G. Ko, S. Ahn, *Adv. Mater.* **2012**, *24*, 1062.
[24] a) J. Y. Ouyang, C. W. Chu, C. R. Szmanda, L. P. Ma, Y. Yang, *Nat. Mater.* **2004**, *3*, 918; b) S. Song, B. Cho, T. W. Kim, Y. Ji, M. Jo, G. Wang, M. Choe, Y. H. Kahng, H. Hwang, T. Lee, *Adv. Mater.* **2010**, *22*, 5048.
[25] C. C. Shih, W. Y. Lee, W. C. Chen, *Mater. Horiz.* **2016**, *3*, 294.
[26] Y. H. Chou, H. C. Chang, C. L. Liu, W. C. Chen, *Polym. Chem.* **2015**, *6*, 341.
[27] H. C. Chang, C. Lu, C. L. Liu, W. C. Chen, *Adv. Mater.* **2015**, *27*, 27.
[28] K. J. Baeg, Y. Y. Noh, H. Sirringhaus, D. Y. Kim, *Adv. Funct. Mater.* **2010**, *20*, 224.
[29] S. T. Han, Y. Zhou, V. A. L. Roy, *Adv. Mater.* **2013**, *25*, 5425.
[30] J. T. Wang, S. Takashima, H.-C. Wu, Y.-C. Chiu, Y. Chen, T. Isono, T. Kakuchi, T. Satoh, W. C. Chen, *Adv. Funct. Mater.* **2016**, *26*, 2695.
[31] B. Ahn, D. M. Kim, J. C. Hsu, Y.-G. Ko, T. J. Shin, J. Kim, W. C. Chen, M. Ree, *ACS Macro. Lett.* **2013**, *2*, 555.
[32] J. C. Chen, C. L. Liu, Y.-S. Sun, S. H. Tung, W. C. Chen, *Soft Matter* **2012**, *8*, 526.
[33] S. Jung, W. Kwon, D. Wi, J. Kim, B. J. Ree, Y. Y. Kim, W. J. Kim, M. Ree, *Macromolecules* **2016**, *49*, 1369.
[34] K. Kim, Y. K. Fang, W. Kwon, S. Pyo, W. C. Chen, M. Ree, *J. Mater. Chem. C* **2013**, *1*, 4858.
[35] K. Kim, Y. Y. Kim, S. Park, Y. G. Ko, Y. Rho, W. Kwon, T. J. Shin, J. Kim, M. Ree, *Macromolecules* **2014**, *47*, 4397.
[36] K. Aissou, I. Otsuka, C. Rochas, S. Fort, S. Halila, R. Borsali, *Langmuir* **2011**, *27*, 4098.
[37] I. Otsuka, Y. Zhang, T. Isono, C. Rochas, T. Kakuchi, T. Satoh, R. Borsali, *Macromolecules* **2015**, *48*, 1509.
[38] I. Otsuka, S. Tallegas, Y. Sakai, C. Rochas, S. Halila, S. Fort, A. Bsiesy, T. Baron, R. Borsali, *Nanoscale* **2013**, *5*, 2637.
[39] J. Cushen, I. Otsuka, C. Bates, S. Halila, S. Fort, C. Rochas, J. Easley, E. Rausch, A. Thio, R. Borsali, G. Willson, C. Ellison, *ACS Nano* **2012**, *6*, 3424.
[40] I. Otsuka, T. Isono, C. Rochas, S. Halila, S. Fort, T. Satoh, T. Kakuchi, R. Borsali, *ACS Macro Lett.* **2012**, *1*, 1379.
[41] N. Raeis Hosseini, J.-S. Lee, *ACS Nano* **2015**, *9*, 419.
[42] N. Raeis-Hosseini, J. S. Lee, *ACS Appl. Mater. Interfaces* **2016**, *8*, 7326.
[43] Y. C. Chiu, H. S. Sun, W. Y. Lee, S. Halila, R. Borsali, W. C. Chen, *Adv. Mater.* **2015**, *27*, 6257.
[44] Y. C. Chiu, I. Otsuka, S. Halila, R. Borsali, W. C. Chen, *Adv. Funct. Mater.* **2014**, *24*, 4240.
[45] H. S. Sun, Y. Chen, W. Y. Lee, Y. C. Chiu, T. Isono, T. Satoh, T. Kakuchi, W. C. Chen, *Polym. Chem.* **2016**, *7*, 1249.
[46] H. S. Sun, Y. C. Chiu, W. Y. Lee, Y. Chen, A. Hirao, T. Satoh, T. Kakuchi, W. C. Chen, *Macromolecules* **2015**, *48*, 3907.
[47] X. H. Dong, W. B. Zhang, Y. Li, M. Huang, S. Zhang, R. P. Quirk, S. Z. D. Cheng, *Polym. Chem.* **2012**, *3*, 124.
[48] H. C. Wu, A. D. Yu, W. Y. Lee, C. L. Liu, W. C. Chen, *Chem. Commun.* **2012**, *48*, 9135.
[49] S. J. Liu, Z. H. Lin, Q. Zhao, Y. Ma, H. F. Shi, M. D. Yi, Q. D. Ling, Q. L. Fan, C. X. Zhu, E. T. Kang, W. Huang, *Adv. Funct. Mater.* **2011**, *21*, 979.
[50] L. H. Xie, Q. D. Ling, X. Y. Hou, W. Huang, *J. Am. Chem. Soc.* **2008**, *130*, 2120.
[51] K. Kim, Y. Y. Kim, S. Park, Y.-G. Ko, Y. Rho, W. Kwon, T. J. Shin, J. Kim, M. Ree, *Macromolecules* **2014**, *47*, 4397.
[52] H. C. Wu, C. L. Liu, W. C. Chen, *Polym. Chem.* **2013**, *4*, 5261.
[53] F. Xu, X. Wang, Y. Zhu, Y. Zhu, *Adv. Funct. Mater.* **2012**, *22*, 1279.
[54] Y. Zhang, C. J. Sheehan, J. Zhai, G. Zou, H. Luo, J. Xiong, Y. T. Zhu, Q. X. Jia, *Adv. Mater.* **2010**, *22*, 3027.
[55] I. Otsuka, K. Fuchise, S. Halila, S. B. Fort, S. K. Aissou, K. I. Pignot-Paintrand, Y. Chen, A. Narumi, T. Kakuchi, R. Borsali, *Langmuir* **2009**, *26*, 2325.
[56] G. Molteni, C. L. Bianchi, G. Marinoni, N. Santo, A. Ponti, *New J. Chem.* **2006**, *30*, 1137.